Journal of the European Ceramic Society 43 (2023) 5014–5025

Contents lists available at ScienceDirect

Journal of the European Ceramic Society

journal homepage: www.elsevier.com/locate/jeurceramsoc

White scheelite-zircon glass ceramic enamels: Clues for their optimization as cool surfaces

Jazmín M. Mayta, Aitana Tamayo *, Berta Pérez, Fausto Rubio, Juan Rubio

Institute of Ceramics and Glass, CSIC, Kelsen 5, 28049 Madrid, Spain

ARTICLE INFO

Keywords:
Solar reflectance
Enamel
Glaze
Crystallization
Urban heat island effect

ABSTRACT

White enamels were prepared from scheelite and zircon glasses. By modifying the amount of WO_3 and ZrO_2, different crystalline shapes and percentages were obtained. It was found that the high refractivity of zircon hinders the crystallization of scheelite and thus the mixture of the two glasses lead to non-crystallized regions which in turn influence the glaze optical properties. In these non-crystallized areas the infrared characterization revealed a large amount of non-bridging oxygens leading to an increase of the band-gap energy and a decrease in the both the solar reflectance and whiteness of the enamels. It was concluded that by reducing the percentage of these non-crystalline regions, the scheelite/zircon glass ceramic enamels could be potential candidates for reducing the Urban Heat Island effect.

1. Introduction

The phenomenon known as the Urban Heat Island effect (UHI) is growing all around the world mainly due to the continuous migration from countryside to cities. This is leading an increased number of transport vehicles, air conditioning systems, gas or electrical heaters, traffic lights, street lamps and other commodities that produce heat during operation. The construction of new factories, buildings, roads, pavements, etc. also contribute to the UHI effect since they contain materials such as asphalt, concrete, metals and brick tiles that are high heat absorbers. It is estimated that urban areas use about 75% of world energy although they occupy only 2% of Earth surface [1]. To that end, several strategies are continuously being developed to mitigate UHI effect. In general, these can be classified as: a) planning new city designs (green spaces, canyons for air flow, green roofs, wind towers, etc., and b) developing passive energy savings systems (solar walls, fenestration, thermal insulation, etc.) [2]. In the strategy of passive energy saving an important effort is been carried out on cool material surfaces, mainly pigments, ceramics, glasses and glass-ceramic materials, retroreflective materials (RR) and phase changed materials (PCM) as well [3]. These cool materials possess the characteristic of presenting high solar reflectance specially in the visible and near infrared regions [4]. These strategies are revealed to reduce air temperature (2 °C), although each solution must be optimized for each urban zone due to the inherent characteristics of each city [5].

With respect to ceramics, glasses and pigments known as cool materials, their main common characteristic is to present a high solar reflectivity in the visible and IR range. In this sense several ceramic pigments with a wide variety of heat absorbing colors (red, blue, pink, yellow, etc.) have been developed [4]. At the same time, ready to use ceramic materials such as roof tiles and pavements with high visible reflectivity are also being developed [6,7] . In the last decade, there have evolved a large number of studies in solar reflective and retroreflective tiles for being installed principally in the Mediterranean area where white or colored surfaces are highly used [7]. These tiles are conformed by a clay substrate containing a thin layer of engobe and on the top surface, a high mechanical resistance layer where the cool ceramic pigments can be incorporated is applied [6,8,9]. In order to obtain the best color results, the engobe layer usually contains important concentrations of zirconium silicate ($ZrSiO_4$) or zirconium derivatives that possess high whiteness this maintaining the optical properties of the top layer deposited afterwards. The top layer, either transparent, opaque matt or glossy, is mainly constituted by a glass or glass-ceramic material known as glaze or enamel [8,9]. For opaque white top layers, the main constituent is also zircon due to its high refraction index (1.94 – 1.96) that leads to a high solar reflectivity of about 80–90% [10]. Zircon can be added as micrometric particles to the whole or it can be grown in situ after a crystallization process during firing and when the top layer is already formed. In this later case, small crystal sizes (in the sub-micrometer range) with spherical and/or needle-like shape are

* Corresponding author.
E-mail address: aitanath@icv.csic.es (A. Tamayo).

https://doi.org/10.1016/j.jeurceramsoc.2023.04.006
Received 17 January 2023; Received in revised form 28 March 2023; Accepted 3 April 2023
Available online 5 April 2023

formed [11,12].

Nevertheless, due to the global price fluctuation of the raw materials (zirconium), different whitening materials are sought to economize the production of reflective materials [13]. Lately, scheelite ($CaWO_4$) has been revealed as strategic material for obtaining high white surface tiles because of its very high refraction index (1.90–1.93) and its special crystallization habit in form of bipyramids of sizes below of 1 μm [14,15]. Scheelite can be easily crystalized by a wide variety of synthetic procedures such as chemical solution [16], co-precipitation [17], sol-gel [18], hydrothermal synthesis [19], sonochemical [20], Czochralski method [21], etc. However, the best method for obtaining well defined bipyramidal crystals has been proved to be through nucleation-crystallization from a silica glass matrix containing calcium and tungsten oxides [15]. In this later case it has been found that if the WO_3 concentration in the glass matrix is close to 6% scheelite crystallizes as a mixture of small bipyramids and long arrows with pyramids at both ends and, with this type of crystallization the tile whiteness reaches 90%.

The aim of this work is to analyse the optical properties of different glass top layers or enamels where scheelite and/or zircon crystals have been grown through a firing treatment where the nucleation-crystallization process is developed. In such enamels the concentrations of WO_3 and ZrO_2 have been chosen for obtaining scheelite and zircon crystals of similar sizes and shapes. The interaction of both enamels has been analysed and their solar reflectance has been determined in order to determine their potential to be used as passive energy savings systems for mitigation the UHI effect, where it is known that through the use of high reflectance surfaces, an energy saving between 10% and 70% can be achieved [22].

2. Experimental section

2.1. Preparation of zircon and scheelite parent glasses

Zircon and scheelite enamels parent glasses (SG: scheelite glass; ZG: zircon glass) were first obtained by melting in a gas furnace. The raw materials (all of them > 99.5% purity) quartz (SiO_2), H_3BO_3, Al_2O_3, $CaCO_3$, Na_2CO_3, K_2CO_3, $MgCO_3$ and ZnO were mixed in a turbula mixer for 4 h and then put in an alumina (Al_2O_3) crucible for calcination at 900 ºC to remove carbonates. The calcined mixtures were melted in a gas furnace at 1450 ºC for 2 h and then poured to a metal plate. The obtained glasses were then crushed and sieved below 100 μm and mixed again with the corresponding amounts of WO_3 or ZrO_2 to achieve the desired chemical concentrations of 6% (wt%). These new compositions were re-melted at 1450 ºC for 2 h and quenched on cold metal plates. The final chemical compositions of both glasses analysed by x-ray fluorescence and ICP-OES are given in Table 1.

2.2. Glaze preparation

The obtaining of the different glaze top coats or enamels was achieved by using the parent glasses or their mixtures. First, SG and ZG were crushed and powdered in an agate mortar to obtain glass particles that were sieved below 100 μm (see Supplementary Material S1). Five different slurries were prepared containing 100 g of the powdered glass (SG, ZG or their mixtures), 30 g H_2O, 7 g $Al_2Si_2O_5(OH)_4$, 2 g carboxymethyl cellulose (CMC, viscosity 50 cp, molecular weight 90,000 g/mol) as binder and 0.5 g of $Na_5P_3O_{10}$ (STPP) as deflocculant. The slurries were thoroughly mixed in an agate jar with agate balls for 15 min at 250 rpm and then they were deposited over porcelain white supports using a tape casting instrument to get coatings of 300 μm thick. No engobe was used in any support. The coated supports were fired at 1170 ºC for 5 min in accordance to a conventional heating cycle using in the tile industry. The percentage of each glass used and labeling of enamel samples is given in Table 2:

2.3. Materials characterization

The chemical compositions were determined by X-ray fluorescence (MagiX, Malvern Panalytcal) and ICP-OES for Boron content (Agilent 700, Agilent Technologies). Hot Stage Microscopy (HSM, EM201 Leica) was used for analysing the viscosity behavior during heating of the as prepared and mixed powders. The Infrared spectra were obtained by an FTIR instrument (Perkin-Elmer, Spectrum BX) using the KBr pellet technique. For this, the enamels were separated from the porcelain tails by using a micro-cutting instrument (Bühler) with a SiC cutting disk and then the extracted fragments were finely powdered in an agate mortar. The powdered enamel powder was mixed with KBr in a 1/300 w/w ratio and pressed at 60 MPa for 3 min. Each spectrum was averaged from 8 collections in the 4000–400 cm^{-1} spectral range with a resolution of 1 cm^{-1} and background subtraction. The Raman spectra were measured in the 1500–100 cm^{-1} spectral range using a 514 cm^{-1} laser excitation in a Renishaw inVia spectrometer focusing the samples with a Leica microscope and 20x objective. The spectra were averaged from 10 collections taken at different locations on the surface of each enamel sample in the HH polarizations (Horizontal transmitting, horizontal receiving) using 90º scattering geometry. UV–VIS–NIR spectra were obtained directly from the surface of each enamel sample in the 280–2500 nm spectral range in a Perkin-Elmer Lambda 950 spectrometer. The instrument was equipped with an integrating sphere for measuring the reflectance of each sample. The corresponding solar reflectance (*SR*, Eq. (1)) was calculated by integrating spectral reflectivity $\rho(\lambda)$ over the whole spectral range (280–2500 nm), and weighted by the direct spectral irradiance of the sun at the earth surface ($SI_{sol,\lambda}$) calculated from ASTM G 173 solar tables [23]. For both variables, $\rho(\lambda)$ and $SI_{sol,\lambda}$ a step size of 5 nm was used.

$$SR = \frac{\sum_{i=300}^{2500} \rho(\lambda_i) SI_{sol,\lambda}(\lambda_i) d\lambda_i}{\sum_{i=300}^{2500} SI_{sol,\lambda}(\lambda_i) d\lambda_i} \quad (1)$$

Color coordinates were acquired by using a CM- 2600d spectrophotometer according to the CIE (International Commission on Illumination) Lab model [24]. Gloss was determined with a Konica Minolta Glossmeter Multi Gloss 268 A. The averaged data (for color and gloss determination) was obtained after measuring at least in five different points randomly distributed over the surface of the enamel sample. For surface roughness characterization an optical profilometer (Zeta-20, Zeta Instruments) was used to calculate the Ra parameter (in microns) by drawing 30 lines on each material piece surface of 30 × 30 mm^2 with a resolution of 13 nm. X-ray diffraction patterns were obtained from the surface of each enamel by employing a Brucker D8 Advance

Table 2
Composition of the mixtures and labeling of the prepared enamels.

Glass / Label	100S	75/25-SZ	50/50-SZ	25/75-SZ	100Z
SG (wt%)	100	75	50	25	0
ZG (wt%)	0	25	50	75	100

Table 1
Chemical composition of the parent glasses (wt%).

	SiO2	B2O3	Al2O3	K2O	Na2O	MgO	CaO	ZnO	WO3	ZrO2
SG	53.8	5.8	8.3	-	8.5	-	10.7	7.2	5.7	-
ZG	55.1	5.3	4.4	3.6	-	2.4	8.9	12.3	-	7.6

diffractometer using Cu $K_{\alpha 1}$ (1.540598 A) radiation and operating at 40 kV. The microstructure of the enamels was observed by a Scanning Electron Microscope (FE-SEM, Hitachi 4700-S). Before observation, the samples were cut and polished with an abrasive SiC paper 1200 grit. The surface analysis of the SEM images was carried out by using the software SigmaScan Pro 5 (Systat Software, Inc.). The obtained pictures were firstly calibrated with the scale bar in the micrography and then, the specific features (crystal sizes, non-crystallized areas, etc.) can be determined by using the designed tool in the software (that accounts pixels for the calibrated length). At least 10 pictures were analysed for each sample.

3. Results

3.1. Structure and microstructure of the enamels

Before enamel preparation, the behavior during heating of the parent SG and ZG glass powders and their mixtures was analysed by means of HSM. The changes in the cross-sectional area (the outline area visible under the HSM) are continuously recorded allowing the calculation of the variation of the sample area via image digital processing being plotted in Fig. 1. This plot allows determining the temperatures that correspond to the fixed points of viscosity [25]. The first fixed point corresponds to the beginning of sintering and is taken from the intercept between the slopes of the first and second HSM stages, whereas the last point (% area-30%) corresponds to a given viscosity where the enamel spreads over the surface of the ceramic support. The other fixed points of viscosity correspond to the end of sintering, softening, sphere, half sphere and one third of sphere. Taken into account these points, the viscosity versus temperature curves were then plotted and given in Supplementary Material S2.

From Fig. 1 it is observed that ZG is the glass most refractory glass presenting the higher sintering temperature while SG sinters at the lowest temperature. As expected, all the SG-ZG mixtures show intermediate sintering temperatures although they are similar to the sintering temperature of SG. In addition, SG glass also presents the lower temperature when it starts spreading over the support (30% area), and the higher temperature corresponds to the 25/75-SZ mixture. A close observation of Fig. 1 reveals that the 75/25-SZ mixture presents a wide range of temperatures with no areal change (870–1070 °C). This behavior appears for the other mixtures although the temperature range decreases as increasing the ZG concentration. The region where the area does not experiment any change with temperature corresponds to the formation of the sphere shape in the HSM. This effect indicates that due to the high refractory behavior of the ZG, the particles of both types of glasses can interact in this interval of temperatures avoiding the reduction of the sample shape and, then it is necessary to apply further heat to start spreading.

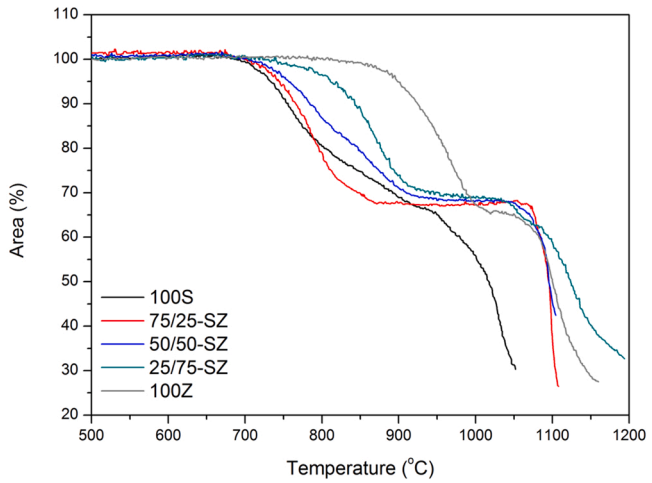

Fig. 1. HSM curves of the different glass powders and their mixtures.

According to HSM curves, the slurries were fired at 1170 °C, i.e. beyond the sphere temperature and when the viscosity is adequate for spreading. The obtained enamels were opaque and white, indicating that the crystallization of scheelite and zircon had occurred [10]. It is known that the crystallization of zircon starts at about 1000 °C and increases very quickly between 1100 and 1200 °C [26] and also the crystallization of scheelite follows a similar behavior [15]. The formation of such crystals was identified by XRD (Fig. 2). In this Fig. 2 the corresponding XRD patters of scheelite (JCPDS 041–1431) and zircon (JCPDS 006–0266) are also plotted. Here it is observed the presence of both types of crystals in the 75/25-SZ; 50/50-SZ, 25/75-SZ enamels and their intensities vary according to the amount of SG and ZG used. Similar XRD patterns have been observed for zircon and scheelite containing glass-ceramic materials [13,15]. In the case of scheelite enamels, the XRD main peak corresponds to the (004) reflection, while in the theoretical pattern is the (112). This fact has been also observed in other works, where scheelite crystallized in silica enamels and, it has been assigned to preferred orientation of scheelite crystals instead of a random orientation on the surface of the enamel [14,15]. On contrary, the main reflection peak of zircon is (200) and this is well observed in all the enamels containing zircon indicating that such crystals do not have grown through any preferential orientation in the enamel. In addition, it can be also observed that in all XRD patterns appear a wide bump (around 25 °θ) due to the presence of a silica glass phase (Supplementary Material S3) [10].

Fig. 3 shows the Raman spectra of the prepared enamels where the peaks associated to the internal modes of scheelite crystals at 911, 837, 796, 400 and 334 cm^{-1} appear [27] as well as those of zircon crystals at 1010, 978, 439, 358 and 226 cm^{-1} [28]. Since the glass structure is strongly polarized, all the Raman spectra were obtained by inserting a polarizer in the scattered beam and measured with parallel polarization. A closer look to the Raman spectra allows distinguishing a wide band attributed to the glassy matrix where the two mentioned phases have evolved as crystals (Supplementary Material S4). The presence of these two crystalline phases within the enamel is in perfect agreement with the XRD results shown in Fig. 2.

In Fig. 4 there are plotted the FTIR spectra of the different enamels. The high bandwidth corroborates the glass nature of the enamels out from where crystallizations have occurred. In these spectra, the band located at 1397 cm^{-1} is assigned to the B-O stretching in BO_3 units and the shoulders around 770 and 700 cm^{-1} are assigned to B-O-B bending vibration of BO_4 groups with W-O-W and in pentaborate groups, respectively [29]. The shoulder located at about 1200 cm^{-1} and the bands close to 1050, 800 and 470 cm^{-1} are due to Si-O-Si bonds [30] whereas the peak at 610 cm^{-1} is assigned to the presence of $ZrSiO_4$ crystals [31]. In the reported spectrum of the scheelite crystals, the most characteristic feature is the band at 800–807 cm^{-1} which is originated from the W–O stretching vibration in the WO_4 tetrahedron [32]. This band is found to be overlapped with the one centered at 800 cm^{-1} (Si-O-Si tetrahedron of the glass matrix) making difficult their entire differentiation. However, the small peak appearing at 795 cm^{-1} in the 100 S sample could be tentatively attributed to the scheelite crystallization. Additionally, in the enamels with high ZG concentration, i.e. samples 100Z and 25/75-SZ, it is possible to appreciate two small shoulders at 970 and 900 cm^{-1} being the first one attributed to Si-O-Zr bonds in the glass structure [33] and the second one to zircon crystals formed in the enamel [31]. In the 50/50-SZ enamel it is only possible to observe the small shoulder around 900 cm^{-1} because of the lower concentration in ZG.

Fig. 5 shows the scheelite and zircon crystals formed in these enamels. In the case of scheelite crystals Fig. 5a) they present an arrow-like shape with pyramids at both ends [15]. There also can be encountered some bipyramids and long arrow-like crystals which are detached

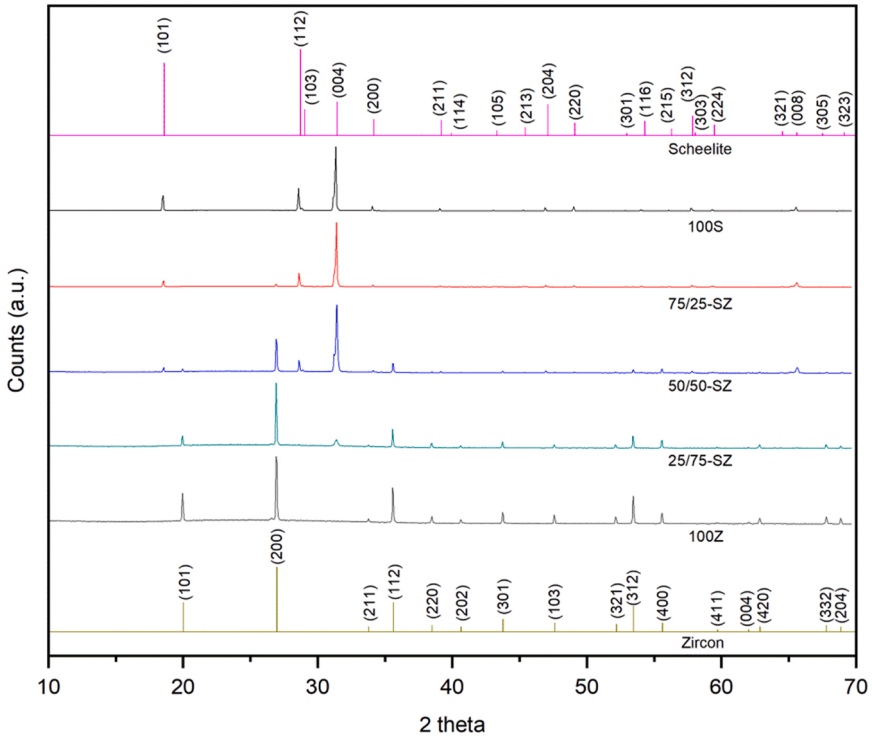

Fig. 2. XRD pattern of the prepared enamels. It is shown the XRD patterns for scheelite and zircon for comparison.

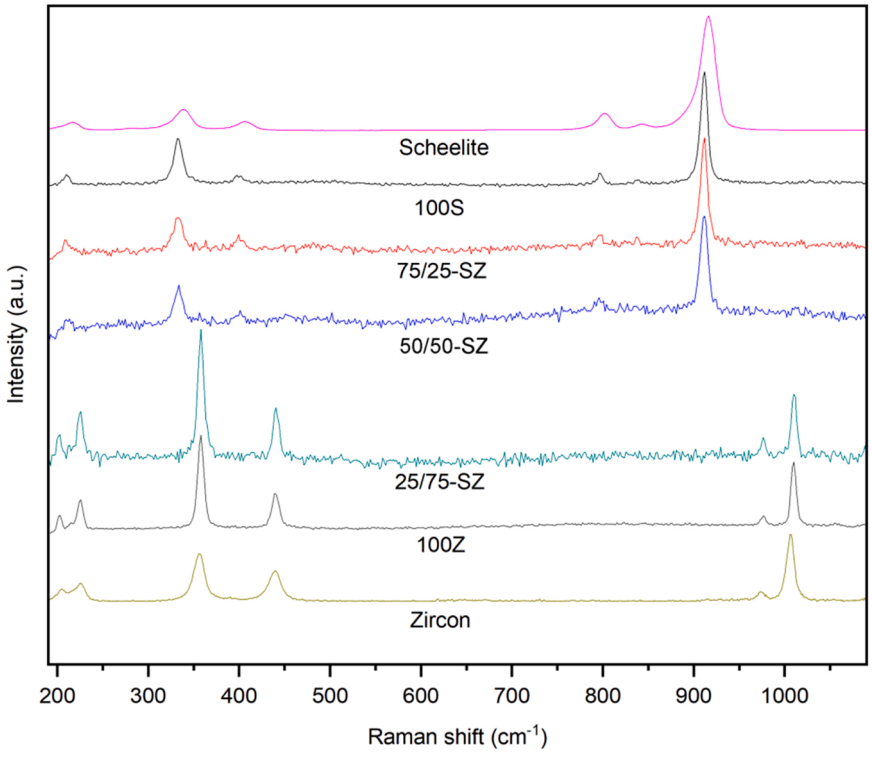

Fig. 3. Raman spectra of the prepared enamels.

to form new bipyramids or new short arrow-like crystals. This behavior was previously described by Taallah et al. in white enamels containing 6% WO_3.[15] On the other hand, the zircon crystals always present their characteristic acicular shape (Fig. 5b) [11].

Fig. 6a-e shows the SEM images corresponding to the microstructures of the different prepared enamels (fresh surface, unpolished material and HF treated for 8 s). There, it can be clearly appreciated the arrow-like scheelite crystals and the acicular shape of the zircon crystals. It is also noticed that the body of the scheelite arrows present a circular cross section (Fig. 6b) whereas the cross section of the zircon crystals (Fig. 6d) is mostly square-shaped.

In the low magnification SEM images (Fig. 7), it is shown that the

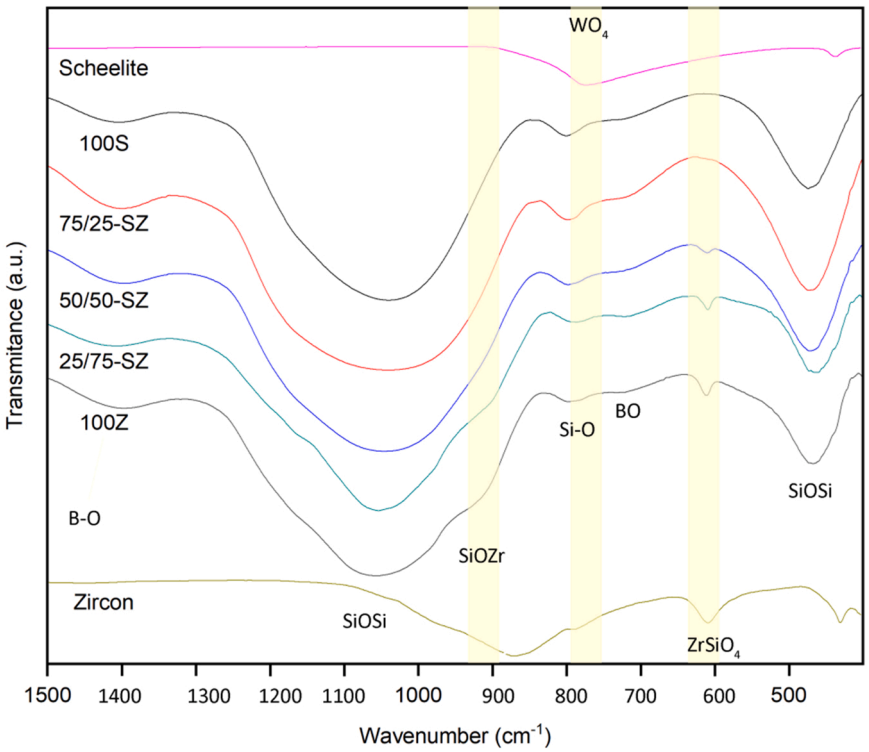

Fig. 4. FTIR spectra of the prepared enamels.

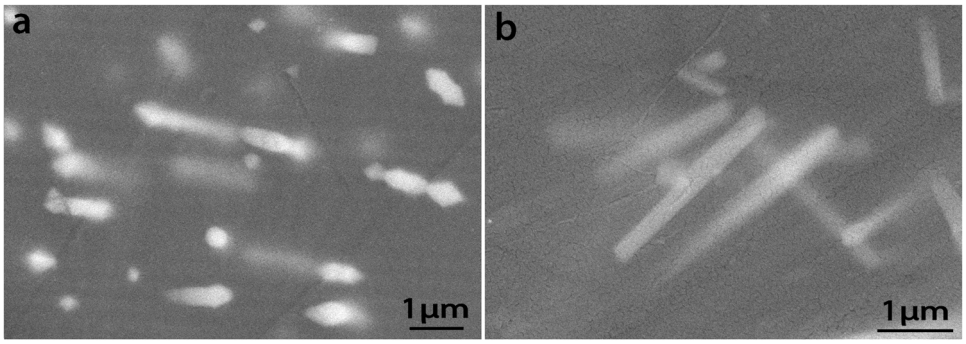

Fig. 5. SEM images of a) scheelite and b) zircon crystals in the enamels.

100 S enamel prepared with only SG glass, shows that the growth of small crystals occurs over the whole bulk material (Fig. 7a). The SEM images shown in Fig. 7b-d correspond to the mixtures of the two parent glasses and it can be appreciated some regions or islands with no crystals. There, it is also observed that the size of such non-crystallized islands is higher for enamel 50/50-SZ followed by the other two mixed enamels (75/25-SZ and 25/75-SZ). In the 100Z enamel shown in Fig. 7e these small areas without crystallizations are also present. A similar observation has been described in several works [12] and has been ascribed to a cluster formation process that occurs during the densification of the glass particles [12].

It is interesting to notice the crystallization habit in the enamels containing the two types of crystals. Fig. 7f shows an enamel area where both scheelite and zircon crystals appear separated with a non-crystallized zone as interface. These images at similar magnifications clearly show the differences between crystallizations. This result and the presence of the above mentioned non crystalline islands indicate that during firing and, probably in the temperature range of 870–1070 °C (where the sphere shape is formed in the HSM, Fig. 1), the glass particles of both SG and SZ glasses interact due to their different viscosity behavior at such temperatures. In such temperature range, the results shown in Fig. 1 demonstrated that while the SG particles tend to soft and flow, ZG only starts sintering thus leading to a restriction in the flow behavior of the SG particles.

The EDX analysis of the materials revealed the actual composition of the crystals. However, it is interesting to analyse the composition of the non-crystallized regions to evaluate if there were compositional differences among enamels (Table 3). The obtained results fit fairly well with the expected chemical composition taking into account the composition of each glass (Table 1) and the inherent inaccuracies of the EDX.

From this Table 3 it can be deduced that despite of the crystallizations observed, there are still some Zr and W remaining in the non-crystallized regions, suggesting that the crystallization could still evolve. Varshneya et al. [34] classified components of the oxide glasses in network formers (GF), such as SiO_2 or WO_3, network modifiers (NM), which are predominantly alkaline and alkaline earth ions, and intermediates, which can act either as GFs and NMs, being the case of Zn, in this study. However, some other studies [35] suggest that some "classical" GFs such as Al_2O_3 or ZrO_2 act in fact as intermediates. It is interesting to compare the relative proportion of NM, (alkaline and

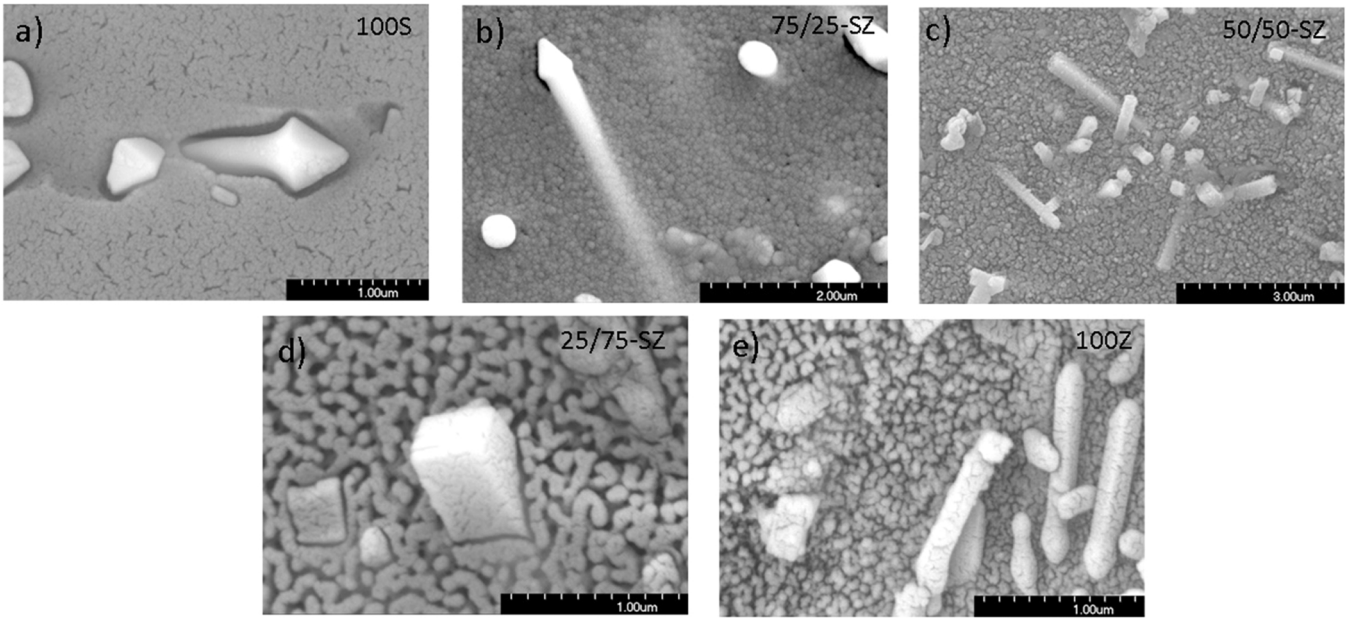

Fig. 6. High magnification SEM images of the unpolished scheelite-zircon enamel samples a) 100S, b) 75/25-SZ, c) 50/50-SZ, d) 25/75-SZ and e) 100Z.

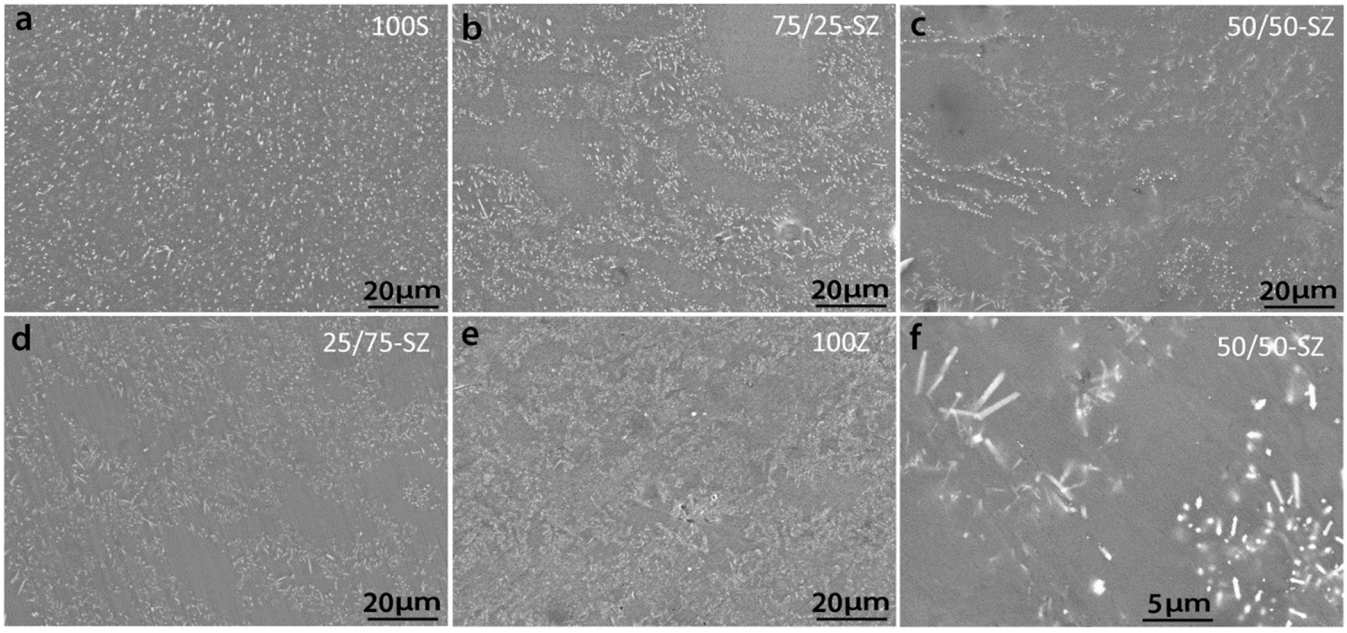

Fig. 7. SEM images of the scheelite-zircon enamels.

Table 3
EDX analysis of the non-crystallized regions of the enamel samples (mol%). NM stands for glass network modifiers and GF stands for glass formers.

	Compound (%)										
Sample	Na_2O	MgO	Al_2O_3	SiO_2	K_2O	CaO	ZnO	ZrO_2	WO_3	NM	GF
100S	7.98		10.39	65.17		7.83	5.74		2.89	16.8	83.2
75/25-SZ	5.27	0.94	8.48	56.01	0.84	10.18	11.76	2.77	3.75	20.2	79.8
50/50-SZ	1.22	0	7.6	65.99	1.65	9.86	9.06	2.77	3.07	14.2	85.8
25/75-SZ	4.23	0	7.34	59.86	1.76	8.89	12.24	1.93	3.77	17.3	82.7
100z	3.89	1.77	5.48	67.31	3.07	3.98	9.85	4.67		14.8	85.2

alkaline earth cations) and GF, being the minimum amount of NM found in the 50/50 composition.

3.2. Optical properties of the enamels

It is widely accepted that the roughness of a surface exerts a large influence on the optical characteristic of the material thus determining not only their reflectance, but gloss, color, etc, as well [36]. The roughness of the prepared enamels was analysed by confocal microscopy over a total length of 6 mm and the Ra values are given in Table 4. The obtained Ra values are characteristic of smooth surfaces. Additionally, similar Ra values were obtained for all the enamel samples prepared independently on the amount of either SG or ZG glasses thus it can be considered that all enamels must be comparable and not influenced by their differentiated roughness [9].

3.2.1. Gloss

Table 4 also gives the obtained gloss values measured at 60º in all the prepared enamels. Gloss values vary between 82 and 92 as correspond to enamels containing more than 6% of zircon [13]. These values are higher than enamels prepared with lower the zircon content [37] and the reported values for enamels that do not contain $ZrSiO_4$ but contain other type of crystals such as anorthite [38] or gahnite [39]. It should be clarified also that similar trends were obtained in the gloss values measured at 20º and 85º.

3.2.2. Color

The L*a*b* values in the visible spectrum are given in Table 4. It is observed that all the prepared enamels present high whiteness (L* >90) due to the presence of scheelite and/or zircon crystals in their bulk structure. Also, b* > a* being always b* > 0, results which are also been encountered in some other reported zircon containing enamels [12,37]. In this Table 4 it is appreciated that L* decreases when the zircon glass concentration increases until a concentration of 50% and then the L* value increases again to reach the maximum value in the 100Z enamel (i.e. 100% of zircon glass). The opposite trend occurs for the b* parameter that increases up to 50% of zircon and then decreases. On the other hand, the a* parameter shows a continue decrease with the zircon glass concentration in the enamel, starting form positive values and reaching a negative value for the 100Z enamel.

3.2.3. Solar reflectance

Fig. 8 shows the obtained UV–vis–NIR for the obtained enamels. It is observed a rapid increase of the reflectance from the UV–vis region to NIR and, in this last region the reflectance remains virtually constant. This behavior has been also observed to occur in some other zircon and scheelite containing enamels [15]. The higher reflectance appears for the 100Z enamel followed by 100 S, indicating a high light diffusion due to the smaller crystal particles existing in these enamels. On the other hand, the reflectance curves of the mixed enamels are dependent on the scheelite-zircon ratio. The average reflectance values in the UV, vis and NIR regions are also collected in Table 4, being those values within the same range as other zircon enamels [12]. According to these values, it can be concluded that the prepared enamels have higher reflectance in the Visible and Near-Infrared regions than in the UV one. Taken into account that the NIR region presents more than the 50% of the total energy spectrum [4] these enamels accomplish the purpose of being used in buildings to mitigate UHI effect [9].

For each reflectance spectrum shown in Fig. 7, In the literature, it has been showed that the addition or crystallization of $ZrSiO_4$ in any enamel leads to an improvement in the SR [7], however the results shown in Table 4 show that SR does not depend on the scheelite/zircon concentration in the enamel and, therefore other factors must be taken into account. The SR values are collected in Table 4 and vary between 74 and 87 with a minimum in the 50/50 concentration. Cool materials are considered to present SR values ranging from 40 to 85 [40] and, therefore the prepared enamels can be considered to belong to this group of materials.

4. Discussion

The experimental results of the prepared enamels and shown in the previous section evidenced the absence of any compositional trend. It has been observed that although both glasses contain WO_3 or ZrO_2 with very similar refraction indexes (1.90–1.93 for scheelite and 1.94–1.96 for zircon) their main properties such as color, gloss and SR are not dependent on the concentrations of SG or ZG glasses in the enamels despite that after crystallization, they present crystals with similar acicular shapes (Figs. 5 and 7). The obtained results indicate that the optical properties are mainly dependent of the microstructure of the materials. According to Table 4, the 100 S enamel has lower values of SR, L* and $R_{average}$ than the 100Z enamel, while gloss and a* and b* values are higher. For the 100 S enamel a* and b* values indicate that there are a little coloration with respect to the 100Z enamel leading to a lower SR and L* values. The high value of gloss for the 100 S enamel with respect to 100Z is probably due to the higher presence of the glassy phase as observed by XRD (see detailed pattern in Supplementary Material S3), Raman (Fig. 3) and SEM results (Fig. 7).

The effect of mixing SG and ZG materials for making scheelite-zircon enamels clearly show a first decrease of SR, L* and $R_{average}$ until the 50/50-SZ composition and then increase to reach values of simple compositions, i.e. 100 S or 100Z. This trend indicates the interaction between the particles of the parent SG and ZG glasses during the formation of the enamels. This interaction has led to changes in the microstructure or in the structure or in both characteristics of the enamels. The microstructures of the obtained enamels of Fig. 7 show that the 100 S enamel presents a homogeneous distribution of scheelite crystals on the bulk material while the 100Z presents some small islands free of zircon crystals. This characteristic of the zircon enamel has been ascribed to the clustering of the $ZrSiO_4$ crystals when the enamel is obtained directly from raw materials but not from a glass frit with the same composition [12] and it has been assigned to the gas release during enamel formation from raw materials because it does not occur if a glass frit is used [12]. In our work there have been exclusively used glass particles, therefore it is not possible to attribute the appearance of these islands to the release of gas during enamel densification implying that other phenomenon takes place.

In accordance with Fig. 7 the crystal clustering leads to island formation appearing in all enamels containing a mixture of zircon and scheelite crystals. The SEM images have been subjected to an imaging

Table 4
Surface properties of the enamel samples.

Sample	Thickness (μm)	Ra (μm)	Gloss	L	a	b	SR	$R_{average}$ (%)			
								UV	Vis	NIR	Total
100S	766	10.29	88	95.0	0.39	1.03	81	56.62	82.44	78.89	78.20
75/25-SZ	394	11.62	89	94.3	0.34	1.88	77	43.65	76.96	78.13	76.09
50/50-SZ	419	11.03	83	93.9	0.22	2.41	74	36.55	73.09	75.08	72.71
25/75-SZ	401	10.70	92	94.9	0.10	1.70	77	49.02	79.48	75.04	74.29
100Z	755	10.43	82	98.9	-0.54	0.88	87	57.82	90.24	83.33	82.96

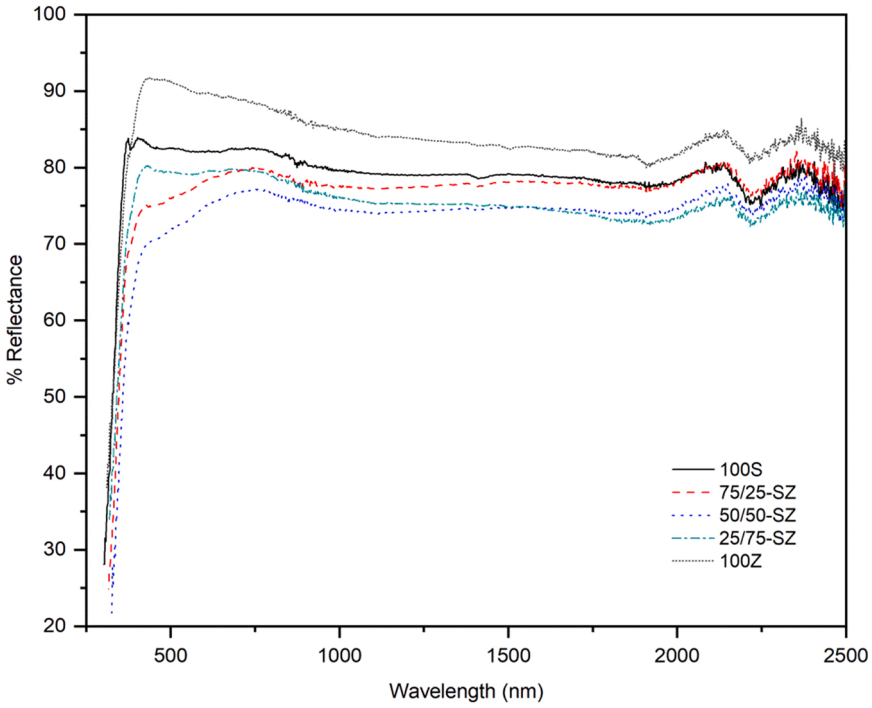

Fig. 8. UV–vis–NIR spectra of the prepared enamels.

Table 5
Percentage area of non-crystallized surface and average parameters of the crystals (calculated from 50% distribution by assuming a Maxwell-Boltzmann distribution, given in Supplementary Material S5).

	Non-Crystallized area (NCA)		Long crystal			Bipyramids		
Enamel	NCA %	sNCA μm^2	Length μm	Diameter μm	L/D –	Long axes μm	Short axes μm	L/D
100S	1	15+/−7	3.44 ± 0.05	0.314 ± 0.03	9.53	0.61 ± 0.20	0.37 ± 0.06	1.65 ± 0.23
75/25-SZ	35	620+/−585	2.57 ± 0.07	0.276 ± 0.03	6.45	0.53 ± 0.10	0.36 ± 0.04	1.47 ± 0.12
50/50-SZ	41	395+/−480	2.66 ± 0.06	0.337 ± 0.02	6.82	0.60 ± 0.18	0.48 ± 0.11	1.25 ± 0.14
25/75-SZ	24	90+/−150	2.65 ± 0.08	0.294 ± 0.02	8.57	-	-	
100Z	14	45+/−45	1.09 ± 0.03	0.225 ± 0.02	4.05	-	-	

analysis, to calculate both the percentage of non-crystallized area (% NCA) with respect to the whole surface, and the average size of the islands, or NCA (sNCA). The obtained results are collected in Table 5.

From the data of Table 5 it can be deduced that the enamel containing only scheelite crystals (100 S) presents a homogeneous distribution of crystals occupying all the analysed surface as it has been shown in Fig. 7, where it is difficult to find NCAs and when present, they are of low size (15 μm^2). The enamel containing only zircon (100Z) presents the above mentioned crystal clustering, also homogeneously distributed in the bulk enamel but, such clustering leaves some small NCAs of a higher percentage (14%) than those of the scheelite enamel. The sizes of the NCA of both enamels are the lowest among all the studied samples (15 μm^2 and 45 μm^2 for 100 S and 100Z, respectively). When SG and ZG are mixed and both types of glass particles crystallize into scheelite and zircon, a high % of NCAs appeared being this percentage higher for the 50/50-SZ enamel (41%). The biggest NCA area is found in the 75/25-SZ enamel (620 μm^2) while in the 25/75-SZ, the NCA decreases in size substantially. The high standard deviation of the NCAs for the mixed enamels indicates a wide distribution with free crystal areas of very different sizes. These results allow corroborate that ZG influences the crystallization process avoiding the formation of scheelite crystals.

Following the same procedure of image analysis, we have analysed the morphological characteristics of the scheelite and zircon crystals. Since in the mixed enamels (75/25-SZ, 50/50-SZ, 25/75-SZ) it is difficult to distinguish between both type of crystals, we have measured all the lengths and diameters of the crystals (independently of their type) and for scheelite bipyramids we have also measured the two axes. The different morphologies of the crystals can be better observed in the SEM images shown on Fig. 6. Fig. 9 shows the distributions of these analyses and the calculated average values by assuming a Maxwell-Boltzmann probability distribution are given in Table 5. From these data it is clear that the arrow-like scheelite crystals present higher lengths and diameters than acicular zircon crystals. The arrow-like scheelite crystals show a wide length distribution (0.1–6.0 μm) and narrow diameter distribution (0.18–0.42 μm) whereas the zircon acicular crystals presents a narrow length distribution (0.1–1.8 μm) and a wide diameter distribution (0.08–0.35 μm). For the mixed enamels it is observed that the distributions of both lengths and diameters are very close to those of scheelite enamel indicating that the zircon crystals probably increase in length and diameter with the presence of the SG particles during the formation of the enamel. The analysis of the bipyramidal axes of scheelite crystals show a small increase in the short axes with the ZG concentration in the enamel. Additionally, by analysing the aspect ratio (Length/Diameter: L/D) of the formed crystals it is observed a lower value for the zircon crystals than scheelite ones and a little influence of the mixed enamels. At the same time, for bipyramid crystals L/D tends to decrease with the ZG concentration in the enamel.

All the above discussion proves the interaction of SG and ZG particles during the formation of all the mixed enamels and the effect produced in

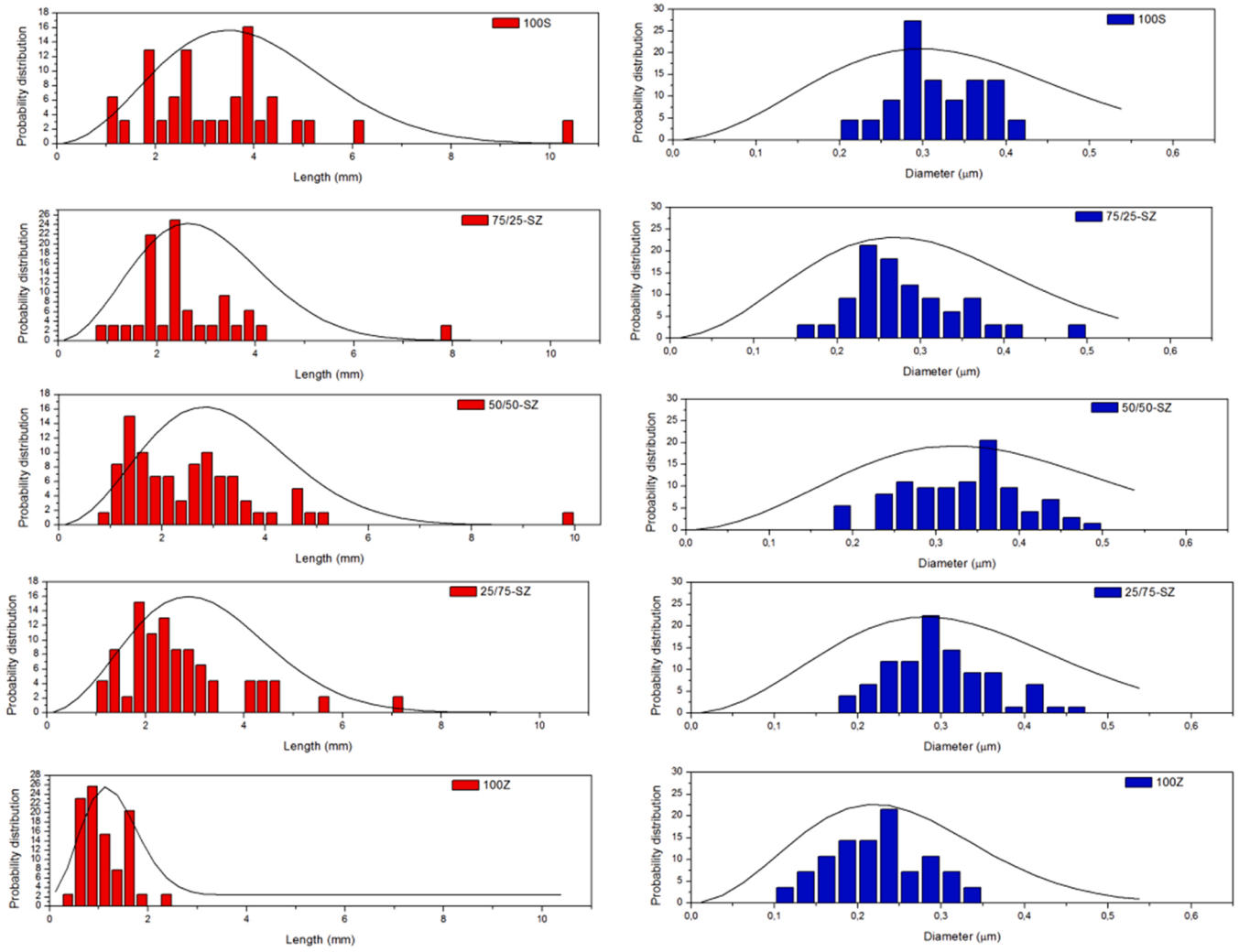

Fig. 9. Size distributions of lengths and diameters of crystals observed in the studied enamels.

the microstructure. This effect leads to prevent the schellite and zircon crystallization and to form large NCAs in the enamel. In these NCAs the absence of crystals in the glass matrix leads to a lower dispersion of the visible light and then a decrease in the solar reflectance and whiteness of the enamels as the results summarized in Table 4 indicate. The analysis of both the glass and crystal structure of glass-ceramic materials is usually carried out by FTIR, Raman and UV–vis–NIR techniques however, the first two techniques give mainly wide bands that are difficult to analyse (see Figs. 3 and 4). To perform a depth analysis of these phases, it is necessary to perform a spectral deconvolution with several Gaussian or Lorentzian shaped bands with ambiguous assignment of widths and positions due to their high overlapping [29]. However, extending the spectroscopic analysis to the UV–vis–NIR range permits to identify some structural changes occurring in the glass network [41]. From UV–vis–NIR spectra the fundamental absorption edge or cut-off [42] and the band-gap energy [43] allows identifying the formation of non-bridging oxygens (NBO) that are created in the glass matrix. In an enamel irradiated with UV–vis–NIR light, when photons enter into the material, they can be absorbed changing the energy states of the atoms taking part of the material structure. Then electrons can move through the conduction to the valence bands if the energy between these bands is sufficiently low to allow the transition stimulated by the energy generated by the photon. The energy difference between conduction and valence band energies, the band gap (E_g), permits characterizing any material when interact with light. The band gap values can be obtained from the UV–vis–NIR reflectance spectra by combining the Kubelka-Munk treatment and Taucś relation [44]:

$$F(R_{\text{inf}}) = A(h\nu E_g)^n / h\nu \quad (2)$$

$$F(R_{\text{inf}}) = (1-R)^2 / 2R \quad (3)$$

where R = reflectance, $h\nu$ = photon energy, A is a constant that depends of the types of transitions indicated by the values of n ($n = 1/2$ or 2 for allowed direct or indirect transitions, respectively, and $n = 3/2$ or 3 for forbidden direct or indirect electronic transitions, respectively). For scheelite and zircon crystals most studies have concluded that the transition type is allowed direct, and then $n = ½$ [45]. On the other hand, for glass materials the analysis of the band-gap is still under consideration because such materials do not present long-range symmetry order and then it is not adequate to use the same approach for crystalline materials to describe the variation of $F(R_{inf})$ with hν [46]. Therefore, since the exact type of transition is unknown, all the possible n values were applied in Eq. (2) because all the values for direct and indirect transitions are normally considered valid for glassy and amorphous materials [47]. By fitting Eq. (3) with the different n values, the optical E_g was obtained by linear extrapolation to $\alpha(h\nu) = 0$. Fig. 10 shows the plots of $\alpha(h\nu)^2$ vs hν for the different enamels and the calculation of the Eg values by extrapolation of the corresponding linear regions in accordance with allowed direct transition (for Indirect transition see Supplementary Material S6).

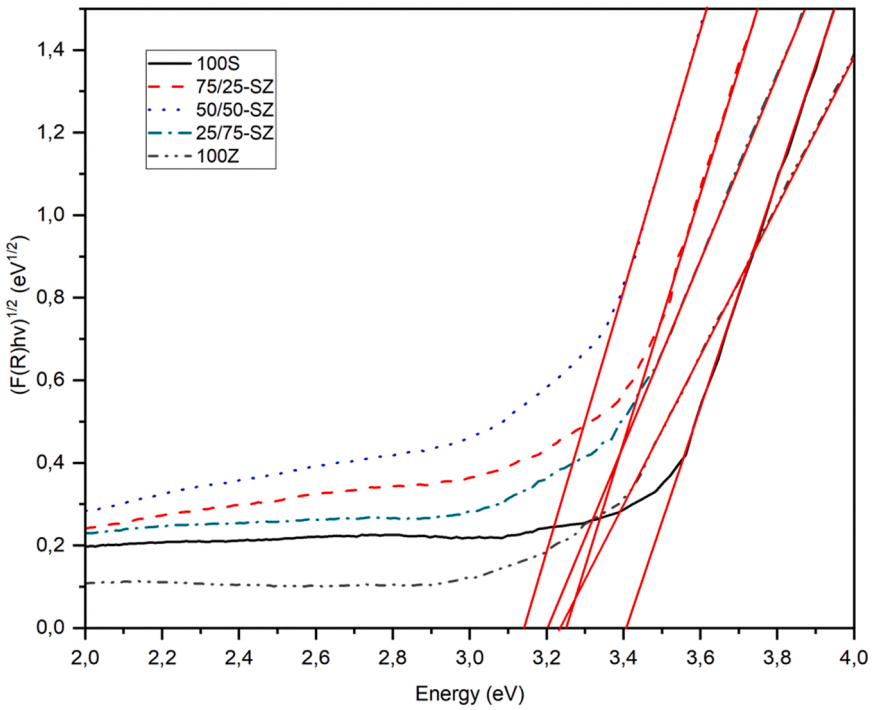

Fig. 10. Plots of α(hν)1/2 vs hν for the obtained enamels.

From theoretical electronic calculations [45] E_g values of 4.09 and 5.69 eV have been obtained for scheelite crystals, while from experimental UV–vis–NIR spectra the reported E_g values varied from 4.2 to 6.8 eV [17]. Similarly, for $ZrSiO_4$ crystals E_g values between 4.43 and 5.9 eV have been obtained [48]. In the case of glasses, the incorporation of metal oxides which act as glass network modifiers produces the weakening of the glass structure due to the formation of NBOs leading to a shift of the band-gap as M. Rodríguez Chialanza et al. have shown [49]. These authors have collected and discussed several works where glasses and crystals with the same compositions present E_g values always lower for the glass materials [49,50]. E_g results collected in Table 6 for direct transition are very close to those found by Srinivasa et al. for Li_2O-Al_2O_3-ZrO_2-SiO_2 glasses with WO_3 concentrations between 1% and 5% [51], while for the 100Z enamel the *Eg* values are very close to those found by Wahab et al. for sodium silicate glasses with ZrO_2 concentrations between 0% and 20% [52]. E_g values for direct and indirect transitions show that the lower value is found for the 50/50-SZ enamel and this must correspond with the large presence of NBOs bonds due to the formation of a higher amount glassy phase and less crystalline material as it was demonstrated in Fig. 7 and Table 5. A clear relationship is found between NCA(%) and E_g (see Supplementary Material S7) but not with its size NCA(s). On the other hand, the cut-off values follow an opposite behavior to E_g being higher for the 50/50-SZ enamel and lower values for the un-mixed enamels. The observed shift towards longer wavelengths has been attributed to the increase in number of the NBOs, a result that coincides with the variation of E_g [53]. The variation of both cut-off and E_g is assigned to the structural changes occurring in the glass enamels as a result of the mixing of different glasses (SG and ZG).

The chemical analysis of the NCA (Table 3) allows estimating the amount of NBO in the NCA. Such as in silicate glasses, each alkaline cation is considered to provide one NBO whereas for alkaline earth cations, each ion will provide two NBO. In the enamel sample 100 S, which shows the lowest cut-off value, the proportion of NBO per mol of GF is estimated to be about 2 mol NBO per mol GF (SiO_2 + WO_3) whereas, in the sample 50/50-SZ, this estimated ratio decreases to about 1/2 mol NBO/mol GF. The general trend, by plotting the cut-off value with the estimated amount of NBO, considering the NM is that the lowest is the amount of NBO, the higher is the cut-off value.

In summary, when different glass particles which crystallize into scheelite or zircon are mixed to obtain glass-ceramic enamels with high whiteness and SR, the interaction between such particles delays the formation of scheelite and zircon crystals leading to remainders of a glass phase in the material. The presence of this glass phase leads to the increase in NBOs with lower *Eg* than the crystalline materials and, the consequent decrease of the whiteness and SR.

Table 6
Bandgap values for the obtained enamels.

Enamel	Cut-off wavelength (nm)	E_g (eV)	
		Direct	Indirect
100S	302	3.97	3.43
75/25-SZ	316	3.85	3.28
50/50-SZ	326	3.76	3.15
25/75-SZ	318	3.90	3.20
100Z	310	3.93	3.24

5. Conclusions

In this work they have been investigated the structural, microstructural and optical properties of different enamels containing scheelite and zircon crystals and their mixtures in order to determine their effect on the solar reflectance and whiteness. These enamels were prepared from the respective parent glasses and they were fired at 1170 °C. The amount of WO_3 and ZrO_2 in the parent glasses was selected to obtain crystals with similar shapes, arrow-like crystals for scheelite and acicular for zircon. For mixed glasses the high refractory behavior of the zircon glass avoids flowing of the less refractory scheelite glass leading to a temperature firing region where the scheelite glass (with lower viscosity) does not spread over the substrate. When the highest firing temperature is reached all glass particles flow and spread over the enamel and also crystallize forming acicular, arrow-like and bipyramids crystals. Such crystallization has been observed by XRD and Raman spectroscopy. While both scheelite and zircon glasses lead to a whole crystallization in the bulk enamel, their mixtures lead to the corresponding crystals and

also to large non-crystallized areas which are higher for the 50–50 mixture. These non-crystallized areas have a glass network structure where the concentration of non-bonding oxygens increases as the cut-off and band-gap results indicated. The formation of these non-crystallized areas leads to changes in the optical properties of the mixed enamels. The lower crystallization decreases both the solar reflectance and whiteness of the enamels and, therefore the mixture of different glasses for obtaining different type of crystals cannot be adequate for increasing the solar reflectance and the mitigation the UHI effect unless these non-crystallized regions are suppressed.

Declaration of Competing Interest

The authors declare that they have no known competing financial interests or personal relationships that could have appeared to influence the work reported in this paper.

Acknowledgments

This work has been developed under the financial support of the project “Fertilizantes Sostenibles Frente al Cambio Global” INCGL20033 framed within the program Plan de Colaboración Internacional from the Spanish National Research Council. The authors acknowledge C. Diaz-Dorado for figures formatting and editing.

Appendix A. Supporting information

Supplementary data associated with this article can be found in the online version at doi:10.1016/j.jeurceramsoc.2023.04.006.

References

[1] E.J. Gago, J. Roldan, R. Pacheco-Torres, J. Ordóñez, The city and urban heat islands: a review of strategies to mitigate adverse effects, Renew. Sustain. Energy Rev. 25 (2013) 749–758.
[2] A.M. Omer, Renewable building energy systems and passive human comfort solutions, Renew. Sustain. Energy Rev. 12 (6) (2008) 1562–1587.
[3] C. Mourou, M. Zamorano, D.P. Ruiz, M. Martín-Morales, Cool surface strategies with an emphasis on the materials dimension: a review, Appl. Sci. 12 (4) (2022) 1893.
[4] S. Jose, D. Joshy, S.B. Narendranath, P. Periyat, Recent advances in infrared reflective inorganic pigments, Sol. Energy Mater. Sol. Cells 194 (2019) 7–27.
[5] J. Yang, Z.-H. Wang, K.E. Kaloush, Environmental impacts of reflective materials: is high albedo a ‘silver bullet’for mitigating urban heat island? Renew. Sustain. Energy Rev. 47 (2015) 830–843.
[6] A.L. Pisello, F. Cotana, L. Brinchi, On a cool coating for roof clay tiles: development of the prototype and thermal-energy assessment, Energy Procedia 45 (2014) 453–462.
[7] C. Ferrari, A. Muscio, C. Siligardi, Development of a solar-reflective ceramic tile ready for industrialization, Procedia Eng. 169 (2016) 400–407.
[8] C. Ferrari, A. Libbra, A. Muscio, C. Siligardi, Design of ceramic tiles with high solar reflectance through the development of a functional engobe, Ceram. Int. 39 (8) (2013) 9583–9590.
[9] C. Ferrari, A. Muscio, C. Siligardi, T. Manfredini, Design of a cool color glaze for solar reflective tile application, Ceram. Int. 41 (9) (2015) 11106–11116.
[10] I. Atkinson, M.E. Smith, M. Zaharescu, Examining correlations between composition, structure and properties in zircon-containing raw glazes, Ceram. Int. 38 (3) (2012) 1827–1833.
[11] L. Schabbach, F. Bondioli, A.M. Ferrari, T. Manfredini, C. Petter, M. Fredel, Influence of firing temperature on the color developed by a (Zr, V) SiO4 pigmented opaque ceramic glaze, J. Eur. Ceram. Soc. 27 (1) (2007) 179–184.
[12] S. Wang, C. Peng, Z. Huang, J. Zhou, M. Lü, J. Wu, Clustering of zircon in raw glaze and its influence on optical properties of opaque glaze, J. Eur. Ceram. Soc. 34 (2) (2014) 541–547.
[13] B. Yildiz, Z. Ozturk, Investigation of the usage of whitening agents as an alternative to zircon in opaque frit compositions, Acta Phys. Pol. A 127 (4) (2015) 1180–1182.
[14] A.F. Gualtieri, L. Canovi, A. Viani, P. Bertocchi, C. Corradini, M.L. Gualtieri, G. C. Gazzadi, M. Zapparoli, S. Berthier, Mechanism of lustre formation in scheelite-based glazes, J. Eur. Ceram. Soc. 33 (11) (2013) 2055–2064.
[15] H. Taallah, A. Chorfa, A. Tamayo, F. Rubio, J. Rubio, Investigating the effect of WO3 on the crystallization behavior of SiO2–B2O3–Al2O3–Na2O–CaO–ZnO high VIS-NIR reflecting glazes, Ceram. Int. 47 (19) (2021) 26789–26799.
[16] L. Xu, Y. Ping, T. Yunfei, L. Yang, X. Dingquan, Synthesis and characterization of nano-calcium tungstate thin film via chemical solution processing, Ferroelectrics 383 (1) (2009) 27–32.
[17] C. Shivakumara, R. Saraf, S. Behera, N. Dhananjaya, H. Nagabhushana, Scheelite-type MWO4 (M= Ca, Sr, and Ba) nanophosphors: facile synthesis, structural characterization, photoluminescence, and photocatalytic properties, Mater. Res. Bull. 61 (2015) 422–432.
[18] Z. Hou, C. Li, J. Yang, H. Lian, P. Yang, R. Chai, Z. Cheng, J. Lin, One-dimensional CaWO 4 and CaWO 4: Tb 3+ nanowires and nanotubes: electrospinning preparation and luminescent properties, J. Mater. Chem. 19 (18) (2009) 2737–2746.
[19] F. Manjón, D. Errandonea, J. López-Solano, P. Rodríguez-Hernández, A. Muñoz, Negative pressures in CaWO 4 nanocrystals, J. Appl. Phys. 105 (9) (2009), 094321.
[20] T. Thongtem, A. Phuruangrat, S. Thongtem, Characterization of MeWO4 (Me= Ba, Sr and Ca) nanocrystallines prepared by sonochemical method, Appl. Surf. Sci. 254 (23) (2008) 7581–7585.
[21] R. Lacomba-Perales, J. Ruiz-Fuertes, D. Errandonea, D. Martínez-García, A. Segura, Optical absorption of divalent metal tungstates: correlation between the band-gap energy and the cation ionic radius, Europhys. Lett. 83 (3) (2008) 37002.
[22] S.E. Bretz, H. Akbari, Long-term performance of high-albedo roof coatings, Energy Build. 25 (2) (1997) 159–167.
[23] A. International, Standard Test Method for Solar Absorptance, Reflectance, and Transmittance of Materials Using Integrating Spheres, Optical Materials for Solar Applications, West Conshohocken, PA, 2020, p. 17.
[24] A. International, Method for Calculation of Color Differences from Instrumentally Measured Color Coordinates, Paint and Related Coatings and Materials, West Conshohocken, PA, 1992, p. 215.
[25] H. Scholze, The influence of viscosity and surface tension on hot-stage microscope measurement of glasses, Glastech. Ber. 39 (1962) 63–68.
[26] S. Wang, C. Peng, M. Lü, J. Wu, Effect of ZnO on crystallization of zircon from zirconium-based glaze, J. Am. Ceram. Soc. 96 (7) (2013) 2054–2057.
[27] M. Liegeois-Duyckaerts, P. Tarte, Vibrational studies of molybdates, tungstates and related compounds—II: new Raman data and assignments for the scheelite-type compounds, Spectrochim. Acta Part A Mol. Spectrosc. 28 (11) (1972) 2037–2051.
[28] R. Syme, D. Lockwood, H. Kerr, Raman spectrum of synthetic zircon (ZrSiO4) and thorite (ThSiO4), J. Phys. C Solid State Phys. 10 (8) (1977) 1335.
[29] M. Farouk, A. Samir, A. Ibrahim, M. Farag, A. Solieman, Raman, FTIR studies and optical absorption of zinc borate glasses containing WO3, Appl. Phys. A 126 (9) (2020) 1–8.
[30] F. Rubio, J. Rubio, J. Oteo, A FT-IR study of the hydrolysis of tetraethylorthosilicate (TEOS), Spectrosc. Lett. 31 (1) (1998) 199–219.
[31] S.-W. Lee, R.A. Condrate, The infrared and Raman spectra of ZrO2-SiO2 glasses prepared by a sol-gel process, J. Mater. Sci. 23 (8) (1988) 2951–2959.
[32] G. Zhang, R. Jia, Q. Wu, Preparation, structural and optical properties of AWO4 (A=Ca, Ba, Sr) nanofilms, Mater. Sci. Eng. B 128 (1) (2006) 254–259.
[33] M. Nogami, Glass preparation of the ZrO2 SiO2 system by the sol-gel process from metal alkoxides, J. Non-Cryst. Solids 69 (2) (1985) 415–423.
[34] A.K. Varshneya, Fundamentals of Inorganic Glasses, Elsevier, 2013.
[35] N. Boubata, A. Roula, I. Moussaoui, Thermodynamic and relative approach to compute glass-forming ability of oxides, Bull. Mater. Sci. 36 (2013) 457–460.
[36] R.C. Veloso, A. Souza, J. Maia, N.M.M. Ramos, J. Ventura, Nanomaterials with high solar reflectance as an emerging path towards energy-efficient envelope systems: a review, J. Mater. Sci. 56 (36) (2021) 19791–19839.
[37] K. Kaczmarczyk, J. Partyka, Effect of ZrSiO4 addition on sintering and selected physicochemical parameters of glass-ceramic materials from the SiO2-Al2O3-Na2O-K2O-CaO-MgO system in the presence of barium oxide, Ceram. Int. 45 (17, Part B) (2019) 22813–22820.
[38] M. Gajek, J. Partyka, A. Rapacz-Kmita, K. Gasek, Development of anorthite based white porcelain glaze without ZrSiO4 content, Ceram. Int. 43 (2) (2017) 1703–1709.
[39] M. Gajek, J. Partyka, M. Leśniak, A. Rapacz-Kmita, Ł. Wójcik, Gahnite white colour glazes in ZnO–R2O–RO–Al2O3–SiO2 system, Ceram. Int. 44 (13) (2018) 15845–15850.
[40] M. Santamouris, A. Synnefa, D. Kolokotsa, V. Dimitriou, K. Apostolakis, Passive cooling of the built environment – use of innovative reflective materials to fight heat islands and decrease cooling needs, Int. J. Low-Carbon Technol. 3 (2) (2008) 71–82.
[41] S.A.A. Wahab, K.A. Matori, S.H.A. Aziz, M.H.M. Zaid, M.M.A. Kechik, A.Z. K. Azman, R.E.M. Khaidir, M.Z.A. Khiri, N. Effendy, Effect of ZnO on the phase transformation and optical properties of silicate glass frits using rice husk ash as a SiO2 source, J. Mater. Res. Technol. 9 (5) (2020) 11013–11021.
[42] D. Singh, K. Singh, G. Singh, Manupriya, S. Mohan, M. Arora, G. Sharma, Optical and structural properties of ZnO–PbO–B2O3 and ZnO–PbO–B2O3–SiO2 glasses, J. Phys. Condens. Matter 20 (7) (2008), 075228.
[43] C. Kittel. Introduction to Solid State Physics, eighth ed., John Wiley & Sons, Inc, 2004.
[44] E.E. Morales, E.S. Mora, U. Pal, Use of diffuse reflectance spectroscopy for optical characterization of un-supported nanostructures, Rev. Mex. Fís. 53 (5) (2007) 18–22.
[45] V.M. Longo, L. Gracia, D.G. Stroppa, L.S. Cavalcante, M. Orlandi, A.J. Ramirez, E. R. Leite, J. Andrés, A. Beltrán, J.A. Varela, E. Longo, A joint experimental and theoretical study on the nanomorphology of CaWO4 crystals, J. Phys. Chem. C 115 (41) (2011), 20113-20119.
[46] J. Singh, Optical Properties of Condensed Matter and Applications, John Wiley & Sons, Ltd, 2006.
[47] N. Ahlawat, A. Agarwal, S. Sanghi, N. Ahlawat, Influence of Ba2+ ions on defect concentration in bismuth silicate glasses evidenced by FTIR and UV–visible spectroscopy, Phys. Status Solidi C, 8(11–12), 2011, pp. 3167–3170.

[48] D.C. Hays, B.P. Gila, S.J. Pearton, B.-J. Kim, F. Ren, Band alignment in ZrSiO4/ZnO heterojunctions, Vacuum 125 (2016) 113–117.
[49] M. Rodríguez Chialanza, R. Faccio, H. Bentos Pereira, R. Marotti, The non-direct band gap in borate glasses; a brief discussion on analysis methodologies and its interpretation, Opt. Mater. 123 (2022), 111890.
[50] I. Hussain, E.K. Barimah, Y. Iqbal, G. Jose, A. Zeb, R. Muhammad, Mechanical and optical properties of ZrO2 doped silicate glass ceramics, Silicon 13 (3) (2021) 877–883.
[51] C.S. Rao, V. Ravikumar, T. Srikumar, Y. Gandhi, N. Veeraiah, The role of coordination and valance states of tungsten ions on some physical properties of Li2O–Al2O3–ZrO2–SiO2 glass system, J. Non-Cryst. Solids 357 (16) (2011) 3094–3102.
[52] E. Wahab, A. Aboraia, A. El Shafey, K.S. Shaaban, A.V. Soldatov, The effect of ZrO2 on the linear and non-linear optical properties of sodium silicate glass, Opt. Quantum Electron. 53 (9) (2021) 1–11.
[53] N. Ahlawat, S. Sanghi, A. Agarwal, S. Rani, Effect of Li2O on structure and optical properties of lithium bismosilicate glasses, J. Alloy. Compd. 480 (2) (2009) 516–520.